Asian Journal of Chemistry; Vol. 26, No. 20 (2014), 6921-6925

ASIAN JOURNAL OF CHEMISTRY

http://dx.doi.org/10.14233/ajchem.2014.17418

Effect of Impurity Concentration on Magnetic Properties of SnO_2 Nanoparticle

M. SARAVANAKUMAR[1,*], S. AGILAN[2], N. MUTHUKUMARASAMY[2], V. RUKKUMANI[3], A. MARUSMY[2] and A. RANJITHA[2]

[1]Department of Physics, SVS College of Engineering, Coimbatore-642 109, India
[2]Department of Physics, Coimbatore Institute of Technology, Coimbatore- 641 014, India
[3]Department of Electronics and Instrumentation, Sri Ramakrishna Engineering College, Coimbatore-641 022, India

*Corresponding author: Fax: +91 422 2321332; E-mail: saranspectra@gmail.com

Received: 19 February 2014; *Accepted*: 17 May 2014; *Published online*: 25 September 2014; AJC-16040

Undoped and Mn doped SnO_2 nanoparticles prepared by co-precipitation method reveal polycrystalline nature with prominent peaks along (110), (101), (211) and (310) planes. All the samples are nanocrystalline with particle size lying in the range of 4.8-5.6 nm calculated by DS formula. As prepared SnO_2 nanoparticles exhibit single tetragonal crystalline phase. The HRTEM results were confirmed by the Scherrer equation using FWHM values of the main peaks in the XRD diffraction pattern. Undoped and Mn doped SnO_2 synthesized successfully confirms by EDAX Spectra. UV-visible absorption and photoluminescence spectroscopy shows the recombination of electrons in singly occupied oxygen vacancies with photoexcited holes in the valence band. UV-visible absorption spectral studies showed a peak at 300 nm. Broad UV emission at 426 nm is observed in photoluminescence spectra of the films along with a blue emission when excited at 385 nm wavelength. Magnetic measurements revealed that all samples exhibit room temperature ferromagnetism, which is identified as an intrinsic characteristics. Pure SnO_2 nanoparticles showed diamagnetism , SnO_2 with lower Mn content show the larger magnetization and with increasing Mn content the ferro magnetization and varies retenivity and coercivity in the range of 0.002-0.014 and 122-183.

Keywords: Mn doped SnO_2 nanoparticles, XRD, EDAX, Optical properties and VSM.

INTRODUCTION

Tin dioxide is a wide band gap n-type semiconductor and is one of the commonly used material for gas sensors, transparent conducting electrodes and opto-electronic devices operating at room temperature[1]. In recent years thin films of SnO_2 have become an integral part of modern electronic technology. Tin dioxide transparent conducting oxide thin film are used as window layers and heat reflectors in solar cells[2]. Semi-conductors with induced magnetization due to doping have an important role in spintronics.

The final properties of impurity doped SnO_2 nanoparticles are related to both composition and processing method. Nano crystalline SnO_2 and Mn doped SnO_2 have been prepared by several methods such as co-precipitation[3], sol-gel[4-6], chemical vapour deposition[7,8], VLS method[9], laser ablation[10] and thermal redox process[11]. Among these methods, chemical co-precipitation method is most effective due to its capability in controlling the structural and surface properties of nanoparticles. In present studies of structural, optical and magnetic properties of undoped SnO_2 and Mn doped SnO_2 nanoparticles, prepared by chemical precipitation are reported.

High temperature ferromagnetism has been reported for Fe doped[12] SnO_2, Cr doped[13] SnO_2, V doped SnO_2 and Ni doped[14,15] SnO_2. Manganese doped SnO_2 was found to be paramagnetic below the tempetature of 5 K[14]. Fitzgerald *et al.*[2] have discussed on the occurrence of ferromagnetism in terms of carrier mediated exchange in spin split impurities band derived from bound magnetic polarons[16] or in a spin split 4s/5s conduction band and then in terms of a model of ferromagnetic ordering of moments of molecular orbitals with 2p hole character, which may be associated with defects in the interface region[17]. It is therefore significant to investigate ferromagnetism in doped and undoped semiconducting or insulating oxide powders because, only powders can reflect intrinsic magnetic properties of the material[18].

The optical properties of semiconductor nanoparticles have recently been a subject of great interest. Semiconductor nanoparticles have been explored as potential electroluminescent materials, with applications in optoelectronics[19]. One approach of producing strongly luminescent nanoparticles is to introduce small quantities of an emissive dopant. Zinc sulfide nanoparticles have been successfully doped with Mn^{2+} and Mn^{2+} emission has been observed following band gap excitation. This emission has been assigned to the $^4T_1 \rightarrow {}^6A_1$ transition of the Mn^{2+} ion[5,20], which is excited by energy transfer from the ZnS electron/hole state. However, with respect to nanocrystalline SnO_2 semiconductor, to the best of our

knowledge, there is no study on the luminescent characteristics of Mn^{2+} doped SnO_2 nanoparticles. Doping influences the photoluminescence of SnO_2 nanoparticles and calcination temperature also affects the luminescence process, which is due to the contribution of oxygen vacancies in the SnO_2 host[21].

For Mn doped SnO_2 nanoparticles, Tian *et al.*[21] reported that magnetic properties strongly depend on both sintering temperature and doping content and no ferromagnetism was observed for samples sintered at a high temperature of 800 °C. Room temperature ferromagnetism with a saturation magnetic moment of 0.18 μB/Mn ion was reported by Gopinadhan *et al.*[17] in Mn doped SnO_2 thin film. Fitzgerald *et al.*[2] reported room temperature ferromagnetism in pulsed laser deposited rutile thin films with 0.1-15 % Mn doping. They observed a large magnetic moment of 20 μB/Mn ion at low doping concentration which is far above the spin magnetic moment of Mn. On the other hand, room temperature ferromagnetism has been reported in undoped SnO_2 nanoparticles[22,23] and thin films[24] containing no intentional magnetic elements as well as in other undoped wide band gap semiconductors and insulators[25-27].

EXPERIMENTAL

All chemicals used in the present work were of analytical grade and were used without further purification. De-ionized water was used in all the synthesis steps. Tin dioxide nano particles doped with three different concentration of Mn, 2, 4 and 6 %, were prepared by chemical co-precipitation sol-gel method. The precursors for dopant and host were manganese acetate tetra hydrate and tin chloride, respectively. The solution was dissolving prepared by tin chloride and manganese acetate tetra hydrate (A.R.) in distilled water to make 0.3 M solution and aqueous ammonia (NH_4OH) of 0.4 M was used as stabilizing agent. The source materials were weighed according to the stoichiometry as per the target compositions and were dissolved in distilled water to make 0.3 M solution. Aqueous solution of ammonia was added drop wise to the solution of tin chloride precursor under continuous stirring for 3 h at room temperature till fine precipitate was formed. Using the same method, we have repeated the procedure for various concentration of $SnCl_2{\cdot}2H_2O$ for molar values of 0.4 and 0.5 M, respectively. The solution obtained was centrifuged at 3000 rpm for 10 min. The precipitate was filtered out separately and washed with de-ionized water to remove the impurities formed during the precipitation process. The obtained product was placed in oven for 8 h at 60 °C.

X-ray diffraction studies have been carried out using PAN alytical X-ray diffractometer. Elemental composition of the prepared samples has been studied using Energy dispersive analysis of X-rays (EDAX, Thermo-Noran system Six). The high resolution transmission electron Microscope (HRTEM) images of the prepared SnO_2 nanoparticles have been recorded using JEOL JEM 2010 microscope. The optical properties have been studied using absorbance spectrum recorded using spectrophotometer (JASCO V-570). Photoluminescence emission spectrum has been recorded using Cary Eclipse spectrophotometer.

RESULTS AND DISCUSSION

Fig. 1 shows the powder XRD patterns of pure and Mn-doped SnO_2 nano particles. All the diffraction peaks are well assigned to the rutile type-tetragonal system of SnO_2 nanoparticles (JCPDS No. 88-0287). The diffraction peaks are observed to shift towards higher angles with increase in Mn content which indicates that Mn ion has substituted for Sn without changing the rutile structure. This is consistent with the reported solubility limit in nano particles[28] and powders[29] of Mn in SnO_2. The observation of peak broadening is due to the occurrence of smaller crystalline size. The crystalline sizes were estimated from the Scherrer's relation[30].

$$D = \frac{K\lambda}{\beta \cos\theta} \quad (1)$$

where, D is the grain size, K is a constant taken to be 0.94, λ is the wavelength of the X-ray radiation, β is the full width at half maximum and θ is the angle of diffraction. The particle size of SnO_2 and Mn doped SnO_2 nanoparticles are found to lie in the range 4.8-5.6 nm (± 0.1 nm). Calculated crystalline size values of pure and Mn doped SnO_2 nano particles are shown in Table-1.

TABLE-1
STRUCUTRAL PARAMETERS OF (A) PURE SnO_2 (B) 2 % Mn DOPED SnO_2 (C) 4 % Mn DOPED SnO_2 (D) 6 % Mn DOPED SnO_2

Materials	2Å (110)	FWHM	a (Å)	Calculated	
				c (Å)	Grain size (nm)
SnO_2	26.45	2.54	4.73	3.19	5.6
2 % Mn doped SnO_2	26.51	2.66	4.71	3.15	5.3
4 % Mn doped SnO_2	26.51	2.73	4.71	3.15	5.2
6 % Mn doped SnO_2	26.77	2.93	4.71	3.15	4.8

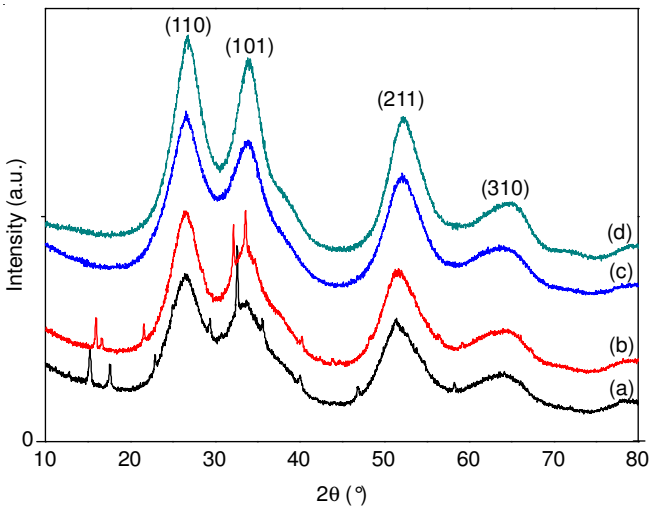

Fig. 1. XRD spectra of (a) pure SnO_2 (b) 2 % Mn doped SnO_2 (c) 4 % Mn doped SnO_2 (d) 6 % Mn doped SnO_2

A small reduction in particle size is observed with increasing Mn concentration. The reduction of the crystallite size suggests that the Mn ion replaces the Sn ion. The presence of Mn ions in the crystallographic structure increases the formation of oxygen vacancies as required by the charge balance.

This effect in conjunction with the smaller ionic radius of Mn^{2+} ion in comparison to Sn^{4+} ion can disturb long range crystallographic ordering, thus reducing the crystallite size. From the diffraction pattern, it is observed that there is no impurities phase such as manganese oxide or other tin oxides are detected.

Fig. 2 shows the HRTEM image, the particles exhibit lattice fringes and using the fringes the d-spacing has been calculated and is found to be 0.35 nm which corresponds to the (110) plane of anatase. From this crystallography, the tetragonal lattice has quadruplicate symmetry. Oxygen atoms (anions) form octahedral and half of the octahedral interstices are filled by Sn atoms[16].

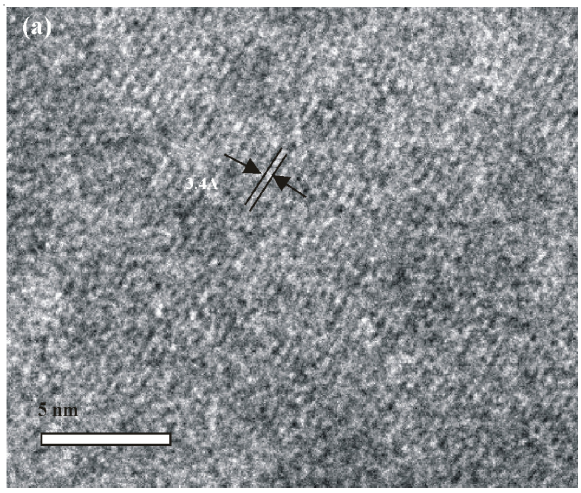

Fig. 2. HRTEM image of Mn doped SnO_2

Fig. 3 shows the EDAX spectra, collected from the average scanned area, of pure SnO_2, and Mn doped (2, 4 and 6 %) SnO_2 samples, respectively. It shows the self generated elemental composition (wt %) details of Sn and O are the only main elemental species in pure SnO_2 sample while, additionally, Mn peaks were observed in Mn doped samples.

Optical studies: Nano sized semiconductor particles generally exhibit a threshold energy in the optical absorption measurements, due to the size-specific band gap structures[31-33], which is reflected by the blue shift of the absorption edge with decreasing particle size. The optical absorption spectra of the samples with three different Mn concentrations (pure 2, 4 and 6 %) are shown in Fig. 4. Pure SnO_2 and Mn doped SnO_2 excitation absorption peak located at 302.05 nm is blue shifted relative to the bulk excitation absorption (300.07 nm). This blue shift indicates the quantum confinement property of nanoparticles. In the quantum confinement range, considering the blue shift of the absorption positions from the bulk SnO_2, the absorption on sets of the present samples can be assigned to the direct transition of electron in the SnO_2 nano crystals. One of the main objectives of the present investigation is to clarify the effect of Mn^{2+} ions on the luminescence for the SnO_2 host.

Fig. 5 shows the excitation and emission spectra of SnO_2/Mn^{2+} samples of different concentration (2, 4 and 6 %) and the pure SnO_2 sample. The excitation spectrum shows one strong band at 420 nm (λ_{em} = 426 nm), which is consistent

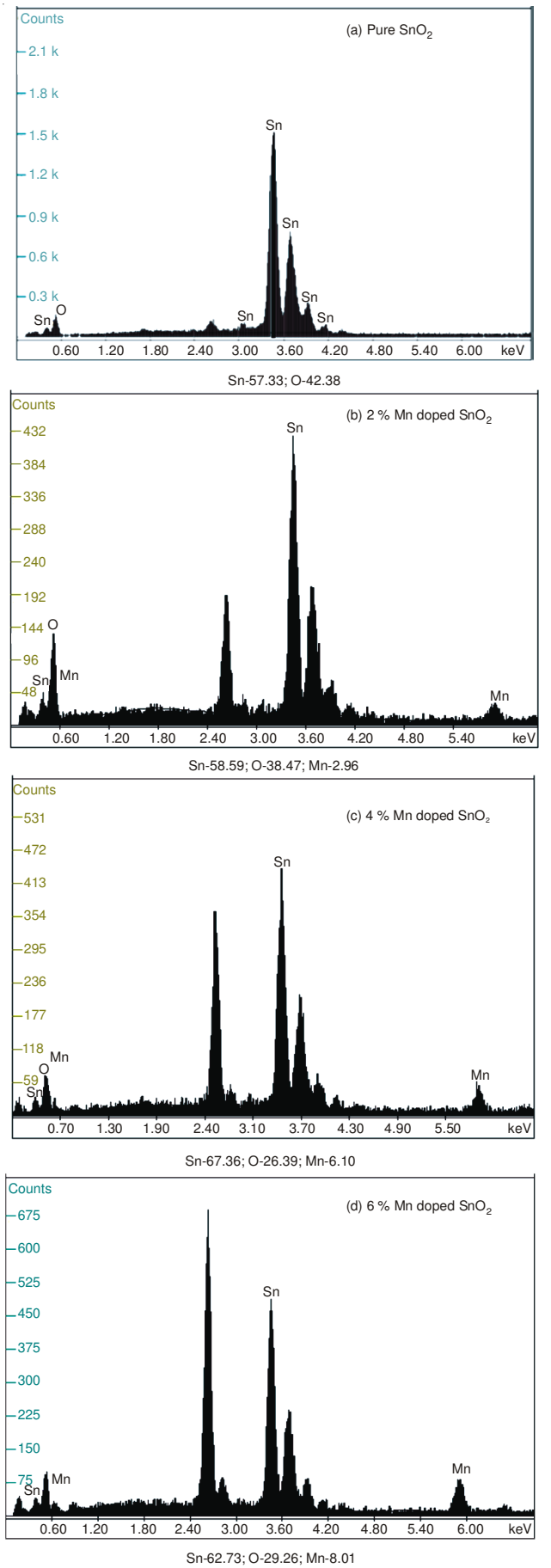

Fig. 3. EDAX spectra of (a) pure SnO_2 (b) 2 % Mn doped SnO_2 (c) 4 % Mn doped SnO_2 (d) 6 % Mn doped SnO_2

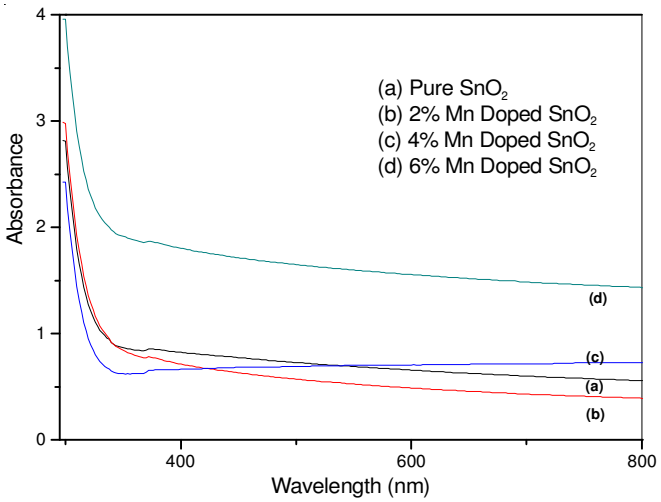

Fig. 4. Absorption spectra of (a) pure SnO_2 (b) 2 % Mn doped SnO_2 (c) 4 % doped SnO_2 (d) 6 % Mn doped SnO_2

with the results of absorption spectra. The emission spectrum is present between bands at 420-430 nm, respectively. From Fig. 5, it can be observed that the addition of Mn^{2+} to SnO_2 host lattice can result in the increment of photoluminescence intensity of SnO_2 host, while the characteristic peaks of Mn^{2+} ions could not be collected, which differs from the behaviour of Mn^{2+} in SnO_2 host. In pure SnO_2 host, the emission attributes to electron transition, mediated by defects levels in the band gap, such as oxygen vacancies, tin interstitials and so forth. Probably after introducing Mn^{2+} into the SnO_2 host, the defects still play a dominant role with respect to the luminescence processes.

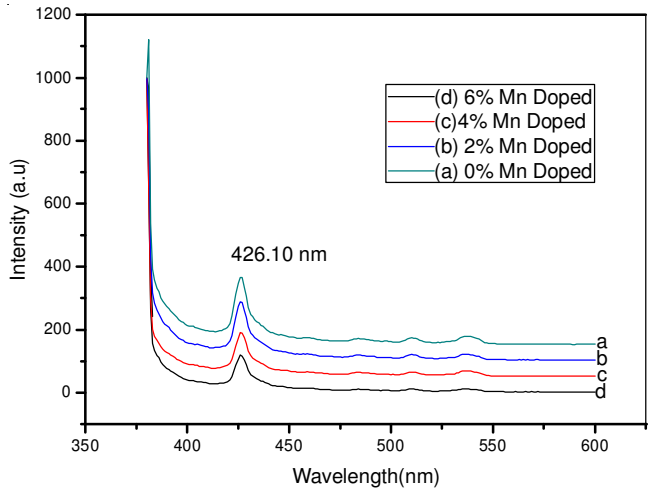

Fig. 5. Excitation and emission spectra of (a) pure SnO_2 (b) 2 % Mn doped SnO_2 (c) 4 % Mn doped SnO_2 (d) 6 % Mn doped SnO_2

Generally, oxygen vacancies are known to be the most common defects and usually act as radiative centers in luminescence processes. The oxygen vacancies present in three different charge states[34]: V_o^0, V_o^+, V_o^2 in the oxide. As V_o^0 is a very shallow donor, the most oxygen vacancies will be in their paramagnetic V_o^+ state under flat-band conditions. And the origin of luminescence is assigned to the recombination of electrons in singly occupied oxygen vacancies with photo-excited holes in the valence band. The temperature behaviour of luminescence spectra of the nano scaled pure SnO_2 powders is similar with those from nanocrystals[35-37] of TiO_2, ZnO and $BaTiO_3$. After the addition of Mn^{2+} to the host lattice, it is easy for Mn^{2+} ion to substitute for Sn^{4+} ion, which can be due to the fact that the radius of Sn^{4+} (0.76 Å) is similar to that of Mn^{2+} (0.80 Å) ion[38]. In addition, the 2+ charge of the Mn_{Sn}^{2-} ion has to be compensated for somewhere in the lattice in the form of oxygen vacancy. That is the reason why the photoluminescence intensity rose rapidly and reached a maximum. At higher Mn^{2+} concentrations, the intensity of the 400 nm peak started to decrease slowly. The similar quenching effect with the Mn^{2+} concentration has been reported previously and it has been a subject of exhaustive studies. Although the exact mechanism for this quenching to occur is still a matter of controversy, it is generally considered that the quenching of the luminescence is associated with interaction among Mn^{2+} ions at the nearest, the second nearest and probably even at the third nearest neighbor sites[39], forming small clusters, such as pairs or triplets, located on the surface or on the grain boundaries of the nano-powders.

Magnetic studies: The magnetic measurements (MeH) of samples at room temperature in the field range of 20 kOe. Fig. 6 shows the hysteresis curves of undoped and Mn doped SnO_2 nano particles. Although undoped SnO_2 nano particles are showing diamagnetism, incorporation of Mn into SnO_2 shows magnetism. The ferromagnetism may be due to the substitution of Mn into SnO_2 lattice or due to the presence of secondary oxide phases of Mn[40]. All the oxides of Mn, only Mn_3O_4 is ferri magnetic with a curie temperature (Tc) of 42 K[41,42]. Since the curie temperature is too low, the observed room temperature ferromagnetic behaviour in the samples cannot be entirely attributed to the Mn_3O_4 phase.

In order to investigate the magnetic properties of the SnO_2 with 2, 4 and 6 % of Mn concentration were studied at room temperature. Pure SnO_2 nanoparticles showed diamagnetism; SnO_2 with lower Mn content (2 %) showed the larger magnetization and with increasing Mn content (4, 6 %), the ferro magnetization diminished (Fig. 6). Here we would like to mention that hysteresis is not observed in the bulk Mn doped SnO_2 samples. The retentivity and coercivity of all samples are calculated and tabulated (Table-2).

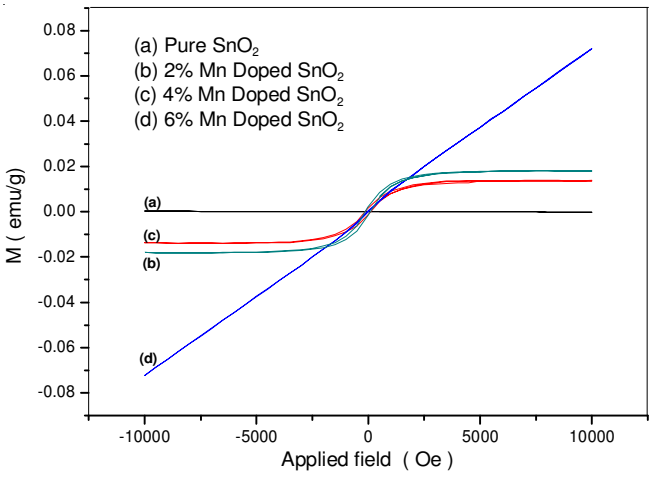

Fig. 6. Hysteresis loop of (a) pure SnO_2 (b) 2 % Mn doped SnO_2 (c) 4 % Mn doped SnO_2 (d) 6 % Mn doped SnO_2

TABLE-2
MAGNETIC PARAMATERS FROM VSM MEASUREMENTS

Material/concentration	Particle size (nm)	Retentivity	Coercivity
Pure SnO_2	5.6	Dia	Dia
2 % Mn doped	5.3	0.002104	122.475
4 % Mn doped	5.2	0.00140	143.962
6 % Mn doped	4.8	0.00035	133.0898

When Mn doping is 2 %, most of the Mn^{2+} ions occupy substitutional position and a few Mn^{2+} ions are oxidized to Mn_3O_4. Mn^{2+} ions, on substitution, create vacancies (as inferred from the appearance of visible emission peaks), those oxygen vacancies alone cannot to contribute to ferromagnetism. Increase of Mn increases the number of oxygen vacancies and therefore an exchange interaction of the Mn ions *via* oxygen vacancies may induce ferromagnetism. Although oxygen vacancies can be expected to be increased at 4 and 6 %, the interaction of Mn^{2+} *via* oxygen vacancies is less pronounced as most of the Mn^{2+} ions form oxide phases. Therefore, it is suggested that both oxygen vacancies and an optimum level of Mn (with entire Mn^{2+} taking part in BMP) are necessary for getting ferromagnetism in Mn doped SnO_2 nanoparticles. The high concentration of Mn does not contribute to ferromagnetism, instead forms secondary oxide phases and contribute to paramagnetism.

Conclusion

Undoped and Mn doped SnO_2 nanoparticles have been successfully prepared by co-precipitation method.The structural and optical properties of pure and Mn doped SnO_2 nanoparticles were studied using XRD and UV-visible. Manganese substitution into the SnO_2 nanoparticles can be confirmed by the shifting of peaks in XRD patterns and shrinkage the lattice constant increasing Mn content. The HRTEM showed that the tetragonal lattice has quadruplicate symmetry. EDAX analysis explained the self generated elemental composition (wt %) details of Sn and O, Mn are the only main elemental species in SnO_2 undoped and Mn doped SnO_2 samples. The shift in E_g could be attributed to the *sp-d* exchange interactions or increase in crystallite size. Sudden decrease in crystallite size could have resulted in blue shift in E_g. In conclusion, it can be suggested that quantum confinement effect dominates the E_g behaviour of Mn doped SnO_2 nanoparticles. Except for the 420 nm emission, all other emissions are suggested to have originated from oxygen defects and induce more defect centered emissions compared to the SnO_2 nanoparticles. Manganese doping resulted in the overall reduction of emission intensity which could be due to non-radiative recombination processes promoted by Mn ions. VSM studies showed high concentration of Mn does not contribute to ferromagnetism, instead forms secondary oxide phases and contribute to paramagnetism.

REFERENCES

1. G. Ansari, P. Boroojerdian, S.R. Sainkar, R.N. Karekar, R.C. Aiyer and S.K. Kulkarni, *Thin Solid Films*, **295**, 271 (1997).
2. C.B. Fitzgerald, M. Venkatesan, L.S. Dorneles, R. Gunning, P. Stamenov, J.M.D. Coey, P. Stampe, R. Kennedy, E. Moreira and U. Sias, *Phys. Rev. B*, **74**, 115307 (2006).
3. M.N. Rumyantseva, V.V. Kovalenko, A.M. Gaskov, T. Pagnier, D. Machon, J. Arbiol and J.R. Morante, *Sens. Actuators B*, **109**, 64 (2005).
4. L. Broussous, C.V. Santilli, S.H. Pulcinelli and A.F. Craievich, *J. Phys. Chem. B*, **106**, 2855 (2002).
5. F. Gu, S.F. Wang, M.K. Lu, Y.X. Qi, G.J. Zhou, D. Xu and D.R. Yuan, *Inorg. Chem. Commun*., **6**, 882 (2003).
6. D. Kotsikau, M. Ivanovskaya, D. Orlik and M. Falasconi, *Sens. Actuators B*, **101**, 199 (2004).
7. S. Suh, Z. Zhang, W. Chu and D.M. Hoffman, *Thin Solid Films*, **345**, 240 (1999).
8. M. Huh, S. Kim, J. Ahn, J. Park and B. Kim, *Nanostruct. Mater*., **11**, 211 (1999).
9. J.H. He, T.H. Wu, C.L. Hsin, K.M. Li, L.J. Chen, Y.L. Chueh, L.J. Chou and Z.L. Wang, *Small*, **2**, 116 (2006).
10. G. Williams and G.S.V. Coles, *Mater. Res. Soc. Bull*., **24**, 25 (1999).
11. O.A. Fouad, *Cryst. Res. Technol*., **41**, 880 (2006).
12. S.B. Ogale, R.J. Choudhary, J.P. Buban, S.E. Lofland, S.R. Shinde, S. Kale, V. Kulkarni, J. Higgins, C. Lanci, J. Simpson, N. Browning, S. Das Sarma, H. Drew, R. Greene and T. Venkatesan, *Phys. Rev. Lett*., **91**, 077205 (2003).
13. J.M.D. Coey, A.P. Douvalis, C.B. Fitzgerald and M. Venkatesan, *Appl. Phys. Lett*., **84**, 1332 (2004).
14. N.H. Hong, J. Sakai, W. Prellier and A. Hassini, *J. Phys. Condens. Matter*, **17**, 1697 (2005).
15. N.H. Hong and J. Sakai, *Physica B*, **358**, 265 (2005).
16. T. Kasuya, *Solid State Commun*., **8**, 1635 (1970).
17. K. Gopinadhan, S.C. Kashyap, D.K. Pandya and S. Chaudhary, *J. Appl. Phys*., **102**, 113513 (2007).
18. V.L. Colvin, M.C. Schlamp and A.P. Alivisatos, *Nature*, **370**, 354 (1994).
19. R.N. Bhargava, D. Gallagher and T. Welker, *J. Lumin*., **60-61**, 275 (1994).
20. R. Bhargava, D. Gallagher, X. Hong and A. Nurmikko, *Phys. Rev. Lett*., **72**, 416 (1994).
21. Z.M. Tian, S.L. Yuan, J.H. He, P. Li, S.Q. Zhang, C.H. Wang, Y.Q. Wang, S.Y. Yin and L. Liu, *J. Alloy. Comp*., **466**, 26 (2008).
22. A. Sundaresan, R. Bhargavi, N. Rangarajan, U. Siddesh and C. Rao, *Phys. Rev. B*, **74**, 161306R (2006).
23. N.H. Hong, N. Poirot and J. Sakai, *Phys. Rev. B*, **77**, 33205 (2008).
24. J.M.D. Coey, M. Venkatesan, P. Stamenov, C. Fitzgerald and L. Dorneles, *Phys. Rev. B*, **72**, 24450 (2005).
25. A. Sundaresan and C.N.R. Rao, *Solid State Commun*., **149**, 1197 (2009).
26. C. Madhu, A. Sundaresan and C. Rao, *Phys. Rev. B*, **77**, 201306R (2008).
27. N.S. Sabri, M.K. Talari, A.K. Yahya, A.K. Yahya and S. Alam, *AIP Conf. Proc*., **1250**, 436 (2010).
28. C. Van Komen, A. Thurber, K.M. Reddy, J. Hays and A. Punnoose, *J. Appl. Phys*., **103**, 7D141 (2008).
29. L.B. Duan, G.H. Rao, J. Yu, Y.C. Wang, G.Y. Liu and J.K. Liang, *J. Appl. Phys*., **101**, 63917 (2007).
30. A. Sharma, M.Varshney, S. Kumar, K.D.Verma and R. Kumar, *Nanomater. Nanotechnol*., **1**, 24 (2011).
31. A. Henglein, *Chem. Rev*., **89**, 1861 (1989).
32. Y. Wang and N. Herron, *J. Phys. Chem*., **95**, 525 (1991).
33. H. Weller, *Adv. Mater*., **5**, 88 (1993).
34. K. Vanheusden, W.L. Warren, C.H. Seager, D.R. Tallant, J.A. Voigt and B.E. Gnade, *J. Appl. Phys*., **79**, 7983 (1996).
35. W.F. Zhang, M.S. Zhang, Z. Yin and Q. Chen, *Appl. Phys. B*, **70**, 261 (2000).
36. W.F. Zhang, M.S. Zhang and Z. Yin, *Phys. Status Solidi*, **179**, 319 (2000).
37. D.W. Bahnemann, C. Kormann and M.R. Hoffmann, *J. Phys. Chem*., **91**, 3789 (1987).
38. D.R. Lide, Handbook of Chemistry and Physics, CRC Press, Boca Raton, FL, edn. 74 (1993).
39. C. Falcony, M. Garcia, A. Ortiz and J.C. Alonso, *J. Appl. Phys*., **72**, 1525 (1992).
40. S. Sharma, S. Chaudhary, S.C. Kashyap and V.K. Malik, *J. Alloys Comp*., **509**, 7434 (2011).
41. Z.M. Tian, S.L. Yuan, Y.Q. Wang, J.H. He, S.Y. Yin, K.L. Liu, S.J. Yuan and L. Liu, *J. Phys. D Appl. Phys.*, **41**, 055006 (2008).
42. S. Sharma, S. Chaudhary, S.C. Kashyap and S.K. Sharma, *J. Appl. Phys*., **109**, 083905 (2011).